

# Fluorescence tomography with simulated data based on the equation of radiative transfer

Alexander D. Klose and Andreas H. Hielscher

Department of Biomedical Engineering & Radiology, Columbia University, ET351 Mudd Building, MC 8904,  
500 West 120th Street, New York, New York 10027

Received November 12, 2002

The quantification of a nonuniform quantum yield or fluorophore absorption distribution is of major interest in molecular imaging of biological tissue. We introduce what is believed to be the first fluorescence image reconstruction algorithm based on the equation of radiative transfer that recovers the spatial distribution of light-emitting fluorophores inside a highly scattering medium from measurements made on the surface of the medium. We obtain images of either the quantum yield or the fluorophore absorption. © 2003 Optical Society of America

OCIS codes: 170.3010, 170.3660, 170.3880, 170.5280, 170.6280, 170.6960.

The advent of many novel biochemical probes that can detect molecular processes that precede the development of diseases promises to bring about fundamental changes in biomedical imaging.<sup>1</sup> Fluorescence imaging makes use of the fact that light-emitting fluorescent probes attach to a specific biological target or emit light when a specific biochemical environment is encountered. One can distinguish two mechanisms that lead to a change in fluorescence signals at certain sites in the body: (1) concentration changes of the fluorophore that are due to preferential uptake or washout in specific tissues and (2) fluorescence quenching due to the biochemical environment that results in changes of quantum yield.<sup>2</sup>

Most work in optical molecular imaging has been limited to direct imaging of fluorescent light that escapes the surface of small animals.<sup>1</sup> In this case, exact localization of light-emitting sources inside the tissue is not possible. Therefore, several groups of researchers have started to develop tomographic image reconstruction schemes that use measured fluorescence signals on the surface of the tissue to determine the spatial fluorescence distribution inside the tissue.<sup>3–8</sup> These imaging algorithms are based on the diffusion model of light propagation in tissue. However, it is well known that the diffusion model is only an approximation to the more generally applicable equation of radiative transfer (ERT). The limits of the diffusion approximation have been well documented.<sup>9–13</sup> For example, the accuracy of this approximation is limited in highly absorbing media, media with small geometries where boundary effects are dominant, and tissue that contains voidlike areas.

In this Letter we introduce what is believed to be the first optical fluorescence image reconstruction model that is based on the ERT. We adapted a model-based iterative image reconstruction scheme that we previously developed.<sup>14,15</sup> This scheme uses a forward model to predict the detector readings on the tissue boundary for a given set of optical parameters. The predicted readings are compared with actual measurements by definition of an appropriate objective function. The objective function is then

minimized by an iterative update of an initial guess of the optical parameters, and the distribution for which the objective function is found to be minimal is displayed as an image.

The light distribution originating from internal fluorescent sources can be described by a forward model consisting of a hierarchical system of two ERTs for the radiance  $\psi(\mathbf{r}, \boldsymbol{\Omega})$  [ $\text{W cm}^{-2} \text{sr}^{-1}$ ], at spatial position  $\mathbf{r}$  and direction  $\boldsymbol{\Omega}$ . Initially an external light source  $S^x$  [ $\text{W cm}^{-3} \text{sr}^{-1}$ ] at wavelength  $\lambda^x$  causes a fluence distribution  $\phi^x(\mathbf{r}) = \int_{4\pi} \psi^x(\mathbf{r}, \boldsymbol{\Omega}) d\boldsymbol{\Omega}$  [ $\text{W cm}^{-2}$ ]. The radiance  $\psi^x(\mathbf{r}, \boldsymbol{\Omega})$  is calculated by the ERT:

$$\begin{aligned} \boldsymbol{\Omega} \cdot \nabla \psi^x + (\mu_a^{x\rightarrow} + \mu_a^{x\rightarrow m} + \mu_s^x) \psi^x \\ = S^x + \mu_s^x \int_{4\pi} p(\boldsymbol{\Omega}, \boldsymbol{\Omega}') \psi^x(\boldsymbol{\Omega}') d\boldsymbol{\Omega}', \quad (1) \end{aligned}$$

with the scattering coefficient  $\mu_s^x(\mathbf{r})$ , the intrinsic absorption  $\mu_a^{x\rightarrow}(\mathbf{r})$  of the tissue, and the absorption  $\mu_a^{x\rightarrow m}(\mathbf{r})$  of the fluorophore. The absorption coefficients can be summed to provide the total absorption  $\mu_a^x(\mathbf{r}) = \mu_a^{x\rightarrow}(\mathbf{r}) + \mu_a^{x\rightarrow m}(\mathbf{r})$ . The fluorophore absorption  $\mu_a^{x\rightarrow m}(\mathbf{r}) = c(\mathbf{r}) \cdot \epsilon$  is linearly proportional to the fluorophore concentration,  $c(\mathbf{r})$ , and the known fluorophore extinction coefficient,  $\epsilon$ . Another important parameter is scattering phase function  $p(\boldsymbol{\Omega}, \boldsymbol{\Omega}')$ , in units of inverse steradians, which accounts for the anisotropic scattering of tissue.

Next, the fluence distribution  $\phi^x(\mathbf{r})$  excites a fluorochrome inside the tissue at position  $\mathbf{r}$ . The excited fluorophore with quantum yield  $\eta(\mathbf{r})$  constitutes an internal source  $S^m(\mathbf{r}, \boldsymbol{\Omega}) = 1/4\pi \eta(\mathbf{r}) \mu_a^{x\rightarrow m}(\mathbf{r}) \phi^x(\mathbf{r})$  and emits light at fluorescence wavelength  $\lambda^m$ . This fluorescent source is isotropic, and its strength depends linearly on the excitation field  $\phi^x(\mathbf{r})$  if saturation and bleaching effects are neglected. Furthermore, the emission source strength is directly proportional to the fluorophore absorption and therefore to the fluorophore concentration. The radiance distribution  $\psi^m(\mathbf{r}, \boldsymbol{\Omega})$  of the fluorescent field is calculated by a second ERT with the optical parameters  $\mu_a^m(\mathbf{r})$  and  $\mu_s^m(\mathbf{r})$  of the fluorescence wavelength  $\lambda^m$ .

$$\mathbf{\Omega} \cdot \nabla \psi^m + (\mu_a^m + \mu_s^m) \psi^m = \frac{1}{4\pi} \eta \mu_a^{x \rightarrow m} \phi^x + \mu_s^m \int_{4\pi} p(\mathbf{\Omega}, \mathbf{\Omega}') \psi^m(\mathbf{\Omega}') d\mathbf{\Omega}'. \quad (2)$$

Both transport equations [Eqs. (1) and (2)] are solved with a finite-difference discrete ordinates ( $S_{\mathcal{N}}$ ) method.<sup>16</sup> The direction  $\mathbf{\Omega}$  is replaced with a set of discrete ordinates  $\mathbf{\Omega}_k$ , and the integral in the ERT is approximated with a quadrature rule:

$$\int_{4\pi} p(\mathbf{\Omega}, \mathbf{\Omega}') \psi(\mathbf{\Omega}') d\mathbf{\Omega}' \approx \sum_{k'=1}^K w_{k'} p(\mathbf{\Omega}_k, \mathbf{\Omega}_{k'}) \psi(\mathbf{\Omega}_{k'}), \quad (3)$$

where  $w_k$  are appropriate weights, determined by full-level symmetry of discrete ordinates.<sup>17</sup> The total number of ordinates  $K$  is given by  $K = \mathcal{N}(\mathcal{N} + 2)$ , where  $\mathcal{N}$  is the number of direction cosines of the  $S_{\mathcal{N}}$  method. The spatial derivatives are substituted with first-order finite-difference approximations known as the step method.<sup>15</sup> The discretized ERTs result in an algebraic system of equations:

$$\mathbf{A}\psi = \mathbf{B}\psi + \mathbf{S}, \quad (4)$$

with  $\mathbf{A}$  as the discretized streaming and collision operator,  $\mathbf{B}$  as the discretized integral operator, and  $\mathbf{S}$  as source term. By considering a source iteration mode,<sup>16</sup> we recast Eq. (4) as

$$\mathbf{A}\psi^{z+1} = \mathbf{B}\psi^z + \mathbf{S} \quad (5)$$

and solve it for radiance  $\psi^{z+1}$  with a Gauss–Seidel method.<sup>15</sup> The predicted detector readings on the boundary at detector position  $\mathbf{r}_d$  are

$$p_d := \phi_d = \int_{\mathbf{n} \cdot \mathbf{\Omega} > 0} \psi(\mathbf{r}_d, \mathbf{\Omega}) d\mathbf{\Omega}, \quad (6)$$

with  $\mathbf{n}$  as the normal vector of the boundary. These predicted readings are used to calculate the objective functions  $\varphi(\mu_a^{x \rightarrow m})$  and  $\varphi(\eta)$  that describe the difference between the measured,  $m_d$ , and predicted,  $p_d$ , data for all  $D$  source–detector pairs:

$$\varphi \approx \sum_{d=1}^D \left( \frac{p_d - m_d}{m_d} \right)^2. \quad (7)$$

In general, the spatial distributions of optical parameters,  $\mu_a^{x \rightarrow m}(\mathbf{r})$  and  $\eta(\mathbf{r})$ , can now be reconstructed by application of a nonlinear optimization technique. We minimize the objective function by using a limited-memory Broyden–Fletcher–Goldfarb–Shanno technique.<sup>18</sup> This method requires the gradient of the objective functions,  $d\varphi/d\mu_a^{x \rightarrow m}$  and  $d\varphi/d\eta$ , which are calculated by means of an adjoint differentiation technique.<sup>15</sup> Once the minimum is found, the final result is the spatial distribution of the optical parameters.

The reconstruction process in optical fluorescence tomography can be performed in two different modes: (A) the fluorescence-contrast mode for reconstructing the quantum yield assuming an accurate reconstruction of the fluorophore absorption or (B) the absorption-contrast mode for reconstructing

the fluorophore absorption assuming a spatially constant quantum yield, which means that no quenching occurs.

We demonstrate in the following examples the feasibility of reconstructing the quantum yield,  $\eta$ , the fluorophore absorption,  $\mu_a^{x \rightarrow m}$ , and its product the fluorescence yield,  $\eta \mu_a^{x \rightarrow m}$ . We generated noise-free measurement data at both wavelengths by employing our forward model. The isotropically scattering medium had a size of  $3 \text{ cm} \times 3 \text{ cm}$  with optical parameters  $\mu_s^x = 10 \text{ cm}^{-1}$  and  $\mu_a^{x \rightarrow} = 0.1 \text{ cm}^{-1}$  at the excitation wavelength and  $\mu_s^m = 10 \text{ cm}^{-1}$  and  $\mu_a^m = 0.1 \text{ cm}^{-1}$  at the emission wavelength. Three fluorescent heterogeneities with a size of  $0.5 \text{ cm} \times 0.5 \text{ cm}$  were embedded inside the medium. Twelve isotropic sources and 88 detectors were equally distributed around the circumference of the medium. The radiance,  $\psi$ , was calculated on a  $61 \times 61$  grid with a  $S_4$  method.<sup>16,17</sup>

First, we investigated the performance of the fluorescence-contrast mode for reconstructing a map of  $\eta$ . The original three fluorescent heterogeneities had all the same fluorophore absorption of  $\mu_a^{x \rightarrow m} = 0.3 \text{ cm}^{-1}$  but different quantum yields, i.e.,  $\eta_1 = 0.08$ ,  $\eta_2 = 0.05$ , and  $\eta_3 = 0.02$  [see Fig. 1(a)]. Different quantum yields are caused by quenching process. The fluorescence-contrast mode was broken up into two steps. First, fluorophore absorption  $\mu_a^{x \rightarrow m}$  at excitation wavelength  $\lambda^x$  was reconstructed by means of Eq. (1), starting from a homogeneous initial guess of  $\mu_a^x = 0.1 \text{ cm}^{-1}$ . Second, the reconstruction of  $\eta$  was performed by means of Eq. (2), where the reconstructed  $\mu_a^{x \rightarrow m}$  distribution of the first step was assumed to be correct and was subsequently included in the source term,  $S^m = 1/4\pi \eta \mu_a^{x \rightarrow m} \phi^x$ . We started the reconstruction from a homogeneous initial guess of  $\eta = 10^{-4}$  and terminated it when the relative difference  $|(\varphi_{n+1} - \varphi_n)/\varphi_n|$  of subsequent iteration steps of the optimization process was smaller than  $\xi = 5 \times 10^{-3}$ . The reconstructed quantum yield  $\eta$  is shown in Fig. 1(b), and the fluorescence yield  $\eta \mu_a^{x \rightarrow m}$  is shown in Fig. 1(c).

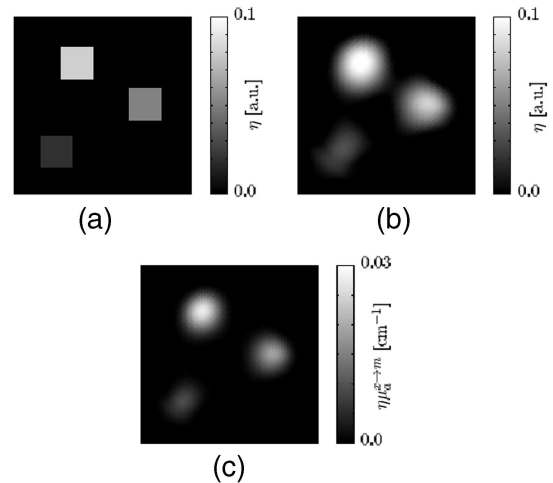


Fig. 1. (a) Original quantum yield distribution  $\eta$ . (b) Reconstructed quantum yield distribution  $\eta$ . (c) Reconstructed fluorescence yield distribution  $\eta \mu_a^{x \rightarrow m}$ .

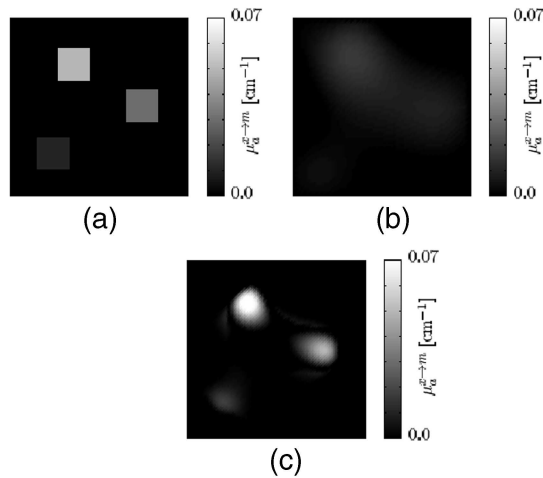


Fig. 2. (a) Original fluorescence absorption  $\mu_a^{x-m}$ . (b) Reconstructed fluorescence absorption  $\mu_a^{x-m}$  by means of Eq. (1). (c) Reconstructed fluorescence absorption  $\mu_a^{x-m}$  by means of Eq. (2).

The image accuracy can be quantified by the error norm,  $\chi = [1/Q \sum_q (\mathcal{O}_q - \mathcal{R}_q)^2 / \sigma]^2$ , where  $Q$  is the number of all image pixels of the original,  $\mathcal{O}$ , and the reconstructed,  $\mathcal{R}$ , image. The standard deviation of the original image is defined as  $\sigma = [1/(Q-1) \sum_q (\mathcal{O}_q - \bar{\mathcal{O}})^2]^{1/2}$ , with  $\bar{\mathcal{O}}$  as the mean value of all pixels. The accuracy of the fluorescence yield map ( $\chi = 0.47$ ) is slightly better than that of the quantum yield ( $\chi = 0.72$ ).

Considering the absorption-contrast mode, we note that the three perturbations had different fluorophore absorption coefficients,  $\mu_{a_1}^{x-m} = 0.05 \text{ cm}^{-1}$ ,  $\mu_{a_2}^{x-m} = 0.02 \text{ cm}^{-1}$ , and  $\mu_{a_3}^{x-m} = 0.01 \text{ cm}^{-1}$  [see Fig. 2(a)], indicating a nonuniform fluorophore concentration. The quantum yield was homogeneously distributed with  $\eta = 0.1$ , therefore no fluorescence quenching was assumed. Again, the reconstruction process was also divided into two stages. First, we reconstructed a map of  $\mu_a^{x-m}$  by means of Eq. (1) as was done in the fluorescence-contrast mode. However, the contrast of the poorly reconstructed  $\mu_a^{x-m}$  image of the first stage [Fig. 2(b),  $\chi = 0.86$ ] can be enhanced by use of Eq. (2) and the fluorescence signal within a second reconstruction process. Thus, only  $\mu_a^{x-m}$  within the source term of Eq. (2) is a spatially varying function, and quantum yield  $\eta$  is kept constant. The reconstructed  $\mu_a^{x-m}$  map of the second stage is shown in Fig. 2(c) ( $\chi = 0.54$ ). We can clearly see a contrast enhancement of the absorption image when the additional fluorescence signal is employed for the reconstruction.

In summary, we have implemented an image reconstruction method based on the equation of radiative transfer that can reconstruct the quantum yield and fluorophore absorption distribution of a highly scattering tissue-like medium. This algorithm promises to provide more-accurate solutions in cases where the diffusion approximation fails, such as in media with small geometries or with high absorption coefficients. More-detailed studies will be necessary to quantify the advantages of the algorithm presented here and to prove its usefulness in clinically relevant problems.

This work was supported in part by a fellowship from the Ernst-Schering Research Foundation, Germany, for A. D. Klose (e-mail: ak2083@columbia.edu.).

## References

1. R. Weissleder and U. Mahmood, *Radiology* **219**, 316 (2001).
2. J. R. Lakowicz, *Principles of Fluorescence Spectroscopy* (Plenum, New York, 1983).
3. M. A. O'Leary, D. A. Boas, X. D. Li, B. Chance, and A. G. Yodh, *Opt. Lett.* **21**, 158 (1996).
4. D. Y. Paithankar, A. U. Chen, B. W. Pogue, M. S. Patterson, and E. M. Sevick-Muraca, *Appl. Opt.* **36**, 2260 (1997).
5. J. Chang, H. L. Graber, and R. L. Barbour, *J. Opt. Soc. Am. A* **14**, 288 (1997).
6. H. Jiang, *Appl. Opt.* **37**, 5337 (1998).
7. V. Ntziachristos and R. Weissleder, *Opt. Lett.* **26**, 893 (2001).
8. M. J. Eppstein, D. J. Hawrysz, A. Godavarty, and E. Sevick-Muraca, *Proc. Natl. Acad. Sci. USA* **99**, 9619 (2002).
9. A. H. Hielscher, R. E. Alcouffe, and R. L. Barbour, *Phys. Med. Biol.* **43**, 1285 (1998).
10. A. D. Kim and A. Ishimaru, *Appl. Opt.* **37**, 5313 (1998).
11. R. Aronson and N. Corngold, *J. Opt. Soc. Am. A* **16**, 1066 (1999).
12. S. R. Arridge, H. Dehghani, M. Schweiger, and E. Okada, *Med. Phys.* **27**, 252 (2000).
13. B. Chen, K. Stamnes, and J. J. Stamnes, *Appl. Opt.* **40**, 6356 (2001).
14. A. H. Hielscher, A. D. Klose, and K. M. Hanson, *IEEE Trans. Med. Imag.* **18**, 262 (1999).
15. A. D. Klose and A. H. Hielscher, *J. Quant. Spectrosc. Radiat. Transfer* **72**, 715 (2002).
16. M. L. Adams and E. W. Larsen, *Prog. Nucl. Eng.* **40**, 3 (2002).
17. B. G. Carlson and K. D. Lathrop, in *Computing Methods in Reactor Physics*, H. Greenspan, ed. (Gordon and Breach, New York, 1968), pp. 166–266.
18. A. D. Klose and A. H. Hielscher, *Inverse Problems* **19**, 387 (2003).